IOP Publishing Journal of Physics D: Applied Physics
J. Phys. D: Appl. Phys. **51** (2018) 015502 (7pp) https://doi.org/10.1088/1361-6463/aa9a74

Effect of notch depth of modified current collector on internal-short-circuit mitigation for lithium-ion battery

Meng Wang[1], Daniel J Noelle[2], Yang Shi[2], Anh V Le[1] and Yu Qiao[1,2]

[1] Department of Structural Engineering, University of California—San Diego, La Jolla, CA 92093-0085, United States of America
[2] Program of Materials Science and Engineering, University of California—San Diego, La Jolla, CA 92093, United States of America

E-mail: yqiao@ucsd.edu

Received 19 July 2017, revised 27 October 2017
Accepted for publication 14 November 2017
Published 8 December 2017

Abstract

Formation of internal short circuit (ISC) may result in catastrophic thermal runaway of lithium-ion battery (LIB). Among LIB cell components, direct contact between cathode and anode current collectors is most critical to the ISC behavior, yet is still relatively uninvestigated. In the current study, we analyze the effect of heterogeneity of current collector on the temperature increase of LIB cells subjected to mechanical abuse. The cathode current collector is modified by surface notches, so that it becomes effectively brittle and the ISC site can be isolated. Results from impact tests on LIB cells with modified current collectors suggest that their temperature increase can be negligible. The critical parameters include the failure strain and the failure work of modified current collector, both of which are related to the notch depth.

Keywords: lithium-ion battery, current collector, internal short circuit, fracture, thermal runaway

(Some figures may appear in colour only in the online journal)

1. Introduction

Among many competing techniques, lithium-ion battery (LIB) is a promising candidate for both transportation and stationary energy storage. Compared to traditional lead-acid batteries and nickel–metal hydride batteries, LIBs have much higher specific energy and energy density [1], as well as excellent service lives [2]. However, system-level and cell-level LIB safety and robustness has become a primary issue. A number of LIB fires and explosions were reported in recent years. For instance, the LIB cells in Boeing 787 [3] and Tesla EVs [4] could catch fire under various thermal and/or mechanical abuse conditions, often associated with thermal runaway.

During normal performance, LIB is well protected by battery thermal management system e.g. [5] and overcharging protection system [6]. When mechanical abuse takes place, e.g. in a traffic accident of EV, external protection may fail. A LIB cell typically comprises of a anode and the cathode, separated by a thin polymer membrane separator. When the cell case is deformed and the thin separator ruptures, the cathode and the anode are forced to contact each other, forming an internal short circuit (ISC). ISC usually leads to rapidly discharge and heat generation. As temperature reaches around 110–150 °C, aggressive exothermic decomposition and reactions of active materials (AMs) and electrolyte begin, which drastically speeds up the heat accumulation rate and finally, may cause thermal runaway [7].

In the past, much research on LIB safety focused on electrical abuse and thermal abuse. External safety devices were developed at the module/pack level. Cell venting valve [8] is an example that releases electrolyte vapor as the inner pressure builds up. Fuses [9] were used as circuit breakers. Nonflammable electrolytes [10] were investigated, yet most of them had negative effects on cell capacity. Electrolyte

additives [11, 12] may help reduce the risk of thermal runaway; but they usually have low voltage limits. Thermal-shutdown separators [13–15] have been widely studied, while they might be insufficient for severe ISC in large-format LIB cells; moreover, if the cell is mechanically damaged and the separator breaks apart, its functionality would be lost. Positive temperature coefficient (PTC) materials [16–18] have a certain operational voltage and temperature ranges, which constraints their applications.

We recently investigated thermal-runaway mitigation mechanisms triggered by mechanical processes. For instance, adding a small amount of damage initiators into electrode [19–21] could promote widespread damages in electrodes under impact. The significant increase in internal impedance could suppress the ISC formation. A major limitation of this work is that, while the microparticulates create cracks in the AM layer, the current collector is still connected. A LIB electrode usually contains an AM layer coated on a current collector. Current collectors are often made of 10–20 μm thick aluminum (Al) or copper (Cu) films. The strength of AM layer is typically only 1–2 MPa [22], and the Al and Cu strength can exceed 60–80 MPa. Thus, while the AM layer is thicker, the current collector accounts for the majority of electrode strength. Furthermore, typical AM conductivity is ~3.8 S m^{-1} [24], and Al and Cu are much more conductive by 4–5 orders of magnitude; thus, current collectors are the most conductive components in LIB and thus should be targeted directly. Formation of ISC through current collectors is a major threat [23–25]. If only AM is separated from an ISC site while the current collectors are still in the circuit, only mild increase in internal impedance may be achieved. We noticed that if the current collector is weakened by heterogeneous features, e.g. surface notches, as the LIB cell is subjected to an external mechanical loading, the ISC sites in current collector may be entirely isolated [26, 27]. This technique has inherent advantages, as it does not affect electrochemical performance of LIB [27] and may be scalable [28]. In the current research, we found that the ISC behavior of modified current collector is heavily dependent on the notch depth. Shallow and deep surface notches may lead to different shorting scenarios, as illustrated in figure 1.

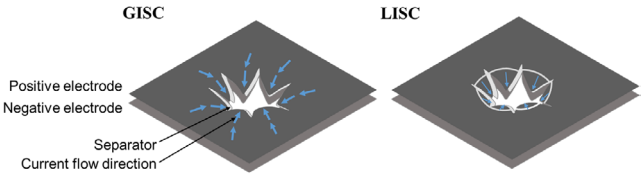

Figure 1. Schematics of two different types of ISC: global internal short circuit (GISC) and localized internal short circuit (LISC).

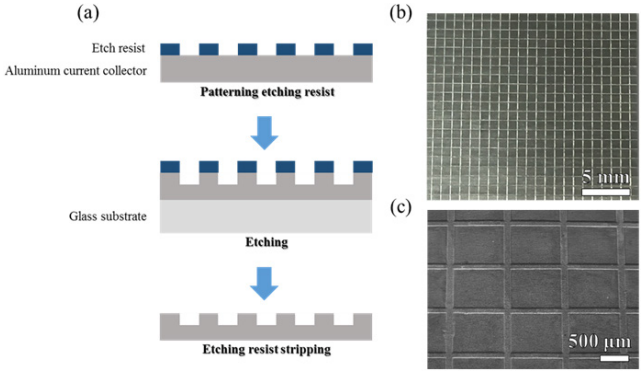

Figure 2. (a) Processing of modified current collector. (b) Photo and (c) SEM image of a modified current collector after etching.

2. Experimental and computer simulation procedures

The processing procedure of surface-notched current collector is summarized in figure 2(a). An 18 μm thick aluminum (Al) sheet was first rinsed with acetone and de-ionized water and dried for 20 min in a vacuum oven at 150 °C. It was then placed onto a 150 μm thick 3 M GG3300 polyester film, and an etching resist layer was printed by a HP Jetpro400 laser printer with the designed pattern. The etching resist layer contained two sets of straight lines perpendicular to each other. In the current study, we focus on testing the notch depth effects, and in all the samples the notch width and spacing were set to be 100 μm and 1 mm, respectively. The coated Al sheet was attached to a 3.2 mm thick glass substrate by using Kapton tapes, and immersed in Transene Type-A Al-Etchant at 50 $\pm$ 1 °C. The temperature was monitored by a type-K thermometer inside the etchant. The etching time varied in the range from 10 min to 20 min. Surface-nothced current collector is shown in figures 2(a) and (b).

The AM in positive electrode was nickel cobalt manganese oxide, NCM532 (Toda America, NCM-04ST). The AM was first mixed in mortar with carbon black (CB) filler nanoparticles (Timcal, C-Nergy Super-C65) and polyvinylidene fluoride (PVDF) binder (Sigma-Aldrich, Product No. 82702) for 30 min. The NCM532-CB-PVDF mass ratio was 93:3:4. Then, 20 wt% 1-Methyl-2-pyrrolidinone (NMP) solvent (Sigma-Aldrich, Product No. 494496) was added and manually mixed in a beaker for 10 min. To increase the uniformity of PVDF and CB distribution, the slurry was homogenized for 15 min by a Qsonica sonicator (Model No. Q55), at the power level of 100%; the homogenization process was stopped for 2 min every 1 min, to avoid over-heating. A reference electrode was produced by coating the slurry onto flat 18 μm thick aluminum current collector with a micrometer adjustable film applicator (MTI, EQ-Se-KTQ-100). The initial coating thickness was around 200 μm. The coated slurry was dried in a vacuum oven for 24 h at 80 °C, and then compacted to the final thickness of ~80 μm by a rolling press. Modified electrodes were processed on surface-notched current collectors through a similar process.

Type-2016 coin cells were fabricated by using the reference or modified electrodes in an argon protection environment (MBraun Glove Box, $H_2O < 0.5$ ppm). Each coin cell comprised of a cathode, a Celgard 2320 membrane separator, and a lithium disc anode, with the diameters of 14.3 mm, 15.9 mm, and 15.6 mm, respectively. After 30 μl BASF electrolyte (1 M $LiPF_6$ in 1:1 EC-EMC) was added into the cathode-separator-anode stack, the coin cell was sealed at 5 MPa in a

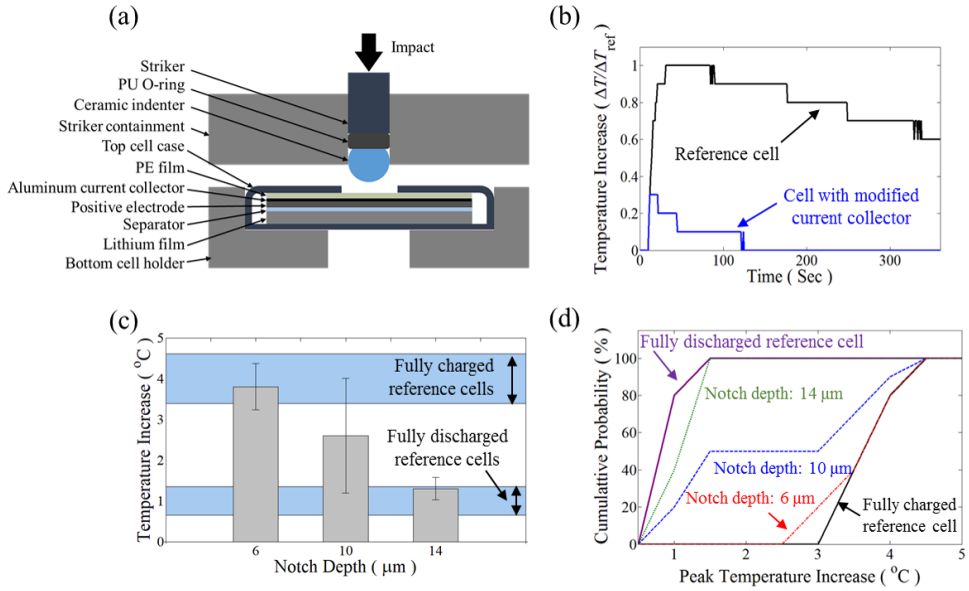

Figure 3. (a) Illustration of the impact test setup. (b) Typical temperature profiles of LIB cells with reference and modified current collectors, where ΔT is the temperature increase and ΔT_{ref} is the temperature increase of reference cell. (c) Relationship between the notch depth and the temperature increase. (d) Probability distribution of temperature increase.

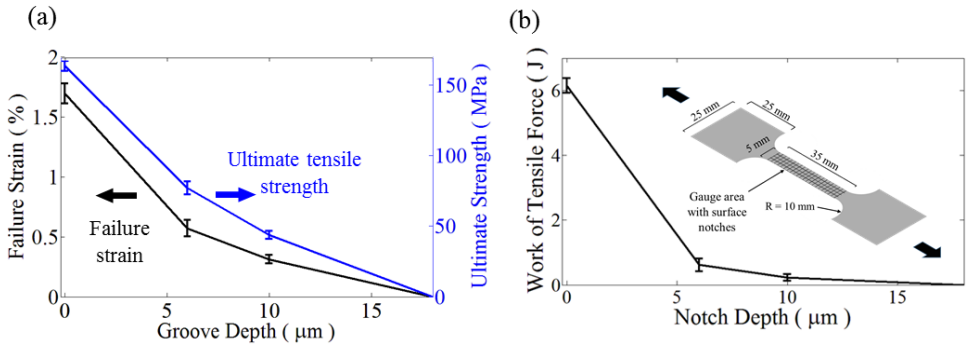

Figure 4. (a) Tensile strength and fracture strain of modified current collector, as functions of notch depth, *D*. (b) Calculated failure work. The inset shows the geometry of tensile specimen.

MTI-MSK-110 hydraulic crimping machine. Before tests, the cells were rest for 12 h, and then charged at C/10 to 4.6 V using a MTI BST8-3 battery analyzer. The charged cell was opened by a MTI CR2016 crimping machine in the glove box and a layer of 150 μm thick polyethylene was added in between the current collector and the cell case, and the initial cell case was replaced by a modified one, with a 6.35 mm diameter opening at the center.

The re-assembled coin cells were used for impact tests, as depicted in figure 3(a). A 4.8 mm diameter ceramic spherical indenter was centered on top surface of the cell, and a 7.8 kg steel cylindrical hammer was dropped at a height of 50 mm. The LIB cell sample was thermally insulated by polyurethane tapes on the top; the bottom of the cell was hosted by a 10 mm thick polyurethane layer. Cell temperature was recorded by an Omega OM-EL-USB-TC temperature logger connected to a type-K thermocouple. The tip of thermocouple was affixed on the top surface of coin cell, ~5 mm to the location of indentation. Testing results are shown in figures 3(b)–(d).

Tensile tests were conducted on surface-notched current collectors by using an Instron 5582 tester; the loading rate was 1 mm min^{-1}. Ultimate tensile strength and failure strain were measured; the total failure work was calculated by integrating the tensile force over the displacement. The results are shown in figure 4. The sample geometry is shown in the inset of figure 4(b).

A finite element (FE) computer simulation model was established. A rigid spherical indenter was placed on a cell case, containing a stack of current collector and lithium anode. The AM layer was ignored, since it contributes little to the electrode strength and stiffness. Three-dimensional eight-node reduced-integration element (C3D8R) was employed for all the components. The current collector, the indenter, the lithium disc, and the cell case were simulated with the mesh sizes of, respectively, 20–40 μm, 160 μm, 160 μm, and 320 μm. Linear elastic-plastic model was adopted for the lithium anode and the steel cell case. The Young's modulus, the Poisson's ratio, the yield strength, and the ultimate tensile strength of the lithium anode were set to 7.8 GPa, 0.36. 0.85 MPa, and 1.38 MPa, respectively. The material model of 304 stainless steel was employed for the cell case, with the Young's modulus and the Poisson's ratio being 197 GPa

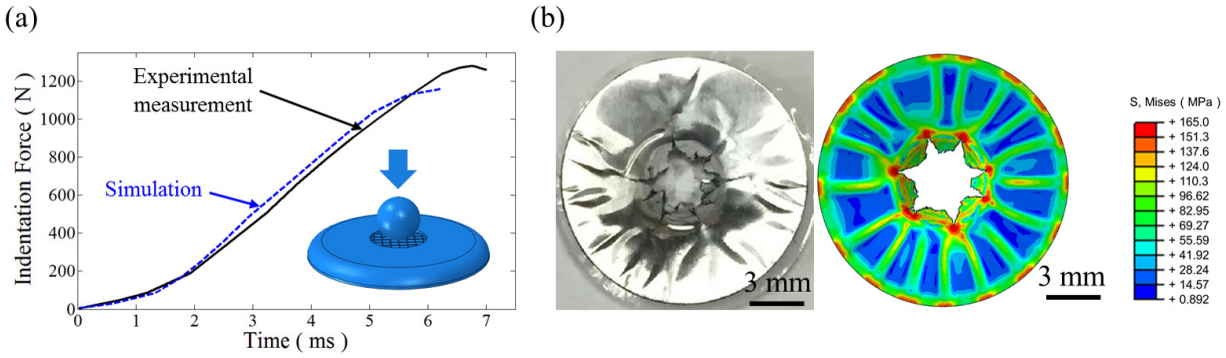

Figure 5. (a) The resistance offered by the battery cell to the indenter. (b) Typical damage mode of tested (left) and simulated (right) pristine current collector.

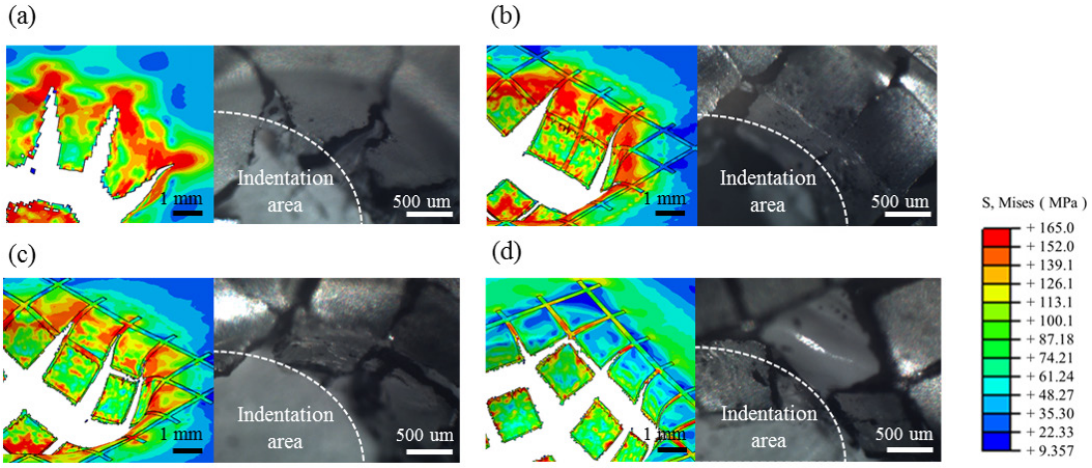

Figure 6. Damage modes of (a) pristine current collector, and modified current collectors with notch depths of (b) 6 μm, (c) 10 μm, and 14 μm, respectively. The initial current collector thickness is 18 μm. The left column is computer simulation results, and the right column is photos of tested samples.

and 0.29, respectively. For the current collector, the damage criterion was defined by the failure strain (ε_f); damaged elements were deleted from the simulation. The current collector was made of 1235-H18 aluminum, with the Young's modulus of 69 GPa and the Poisson's ratio of 0.33; the yield strength and the ultimate tensile strength are 151 MPa and 165 MPa, respectively. The failure strain of current collector was 2%, according to our tensile tests (figure 4(a)). FE analysis results are compared with experimental data, as shown in figures 5 and 6. Figure 7 shows the FE prediction of crack propagation under various scenarios.

3. Discussion

The relationship between the etching time and the notch depth of modified current collector is nonlinear. When the etching times are 10 min, 15 min, and 20 min, the notch depths are 6 μm, 10 μm, and 14 μm, respectively. The scatter in notch depth is ± 1 μm. Depending on whether the current collector contains heterogeneous surface notches and how deep the notches are, the behaviors of the coin cells in impact tests are different. Two primary failure modes of electrodes are identified: global ISC (GISC), which occurs in reference coin cells based on pristine current collectors; and localized ISC (LISC), which occurs when the notches in current collector are sufficiently deep. When the notches are relatively shallow, the failure of electrodes exhibits mixed characteristics of GISC and LISC.

As depicted in figure 1, in the GISC mode, the indenter intrudes into the coin-cell case and deforms the electrode. While a large number of radial and circular cracks are generated in the AM layer, the cracks in the ductile current collector are mainly along radial directions (figure 6(a)). The petals in between radial cracks are bent and penetrate through the thin separator, in direct contact with the lithium disc anode—This is a typical scenario of ISC formation. As a result, the stored electric energy of the entire electrode is rapidly released as heat. In the forward path of ISC, i.e. the deformed current collector petals, electrons move from the anode layer to the cathode layer; in the return path surrounding the ISC site, lithium ions (Li^+) move through the electrolyte. Due to the high energy density, the heat generation is fast. For the coin cells under investigation, because of the large surface area-to-volume ratio, the temperature increase, ΔT, is only a few °C; in a large pouch cell, ΔT can be a few hundred °C [23]. When the electric energy is consumed, the heat generation rate starts to decrease; and as ΔT rises, the heat transfer rate increases.

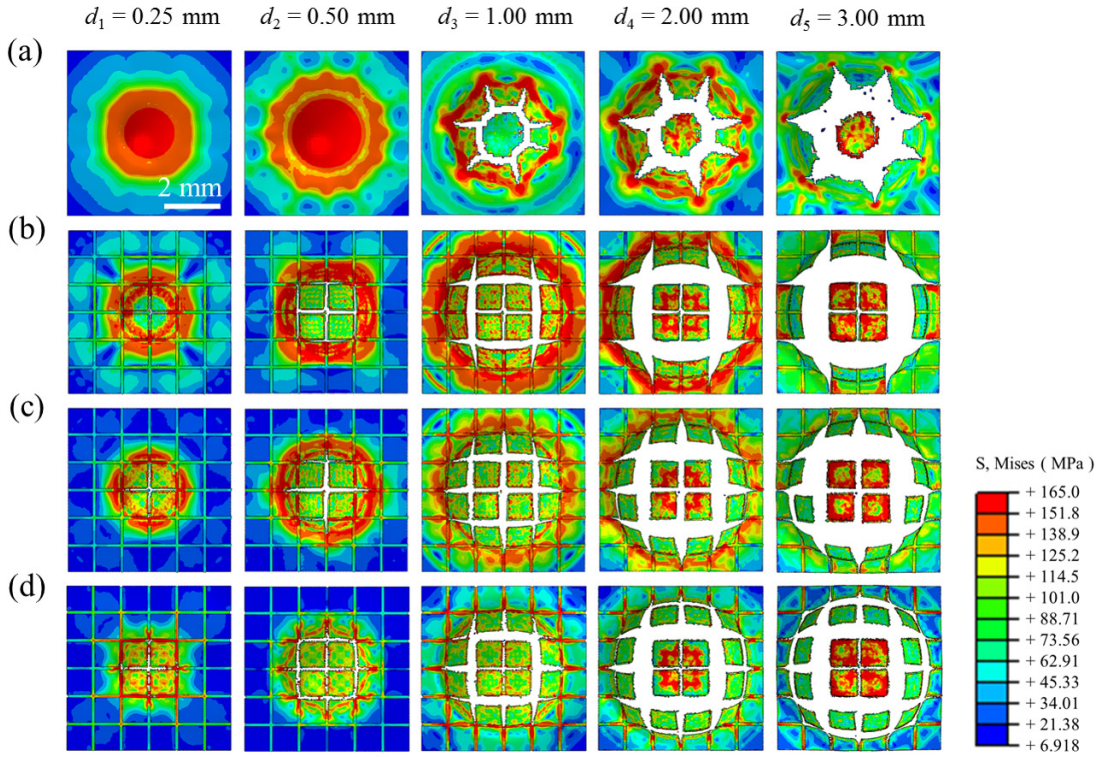

Figure 7. Evolution of cracks in (a) pristine current collector, and modified current collectors with notch depths of (b) 6 μm, (c) 10 μm, and 14 μm, respectively. The color indicates the Mises stress and d_i (i = 1,2,…5) is the indentation displacement.

Eventually, in ~30 s, ΔT reaches the peak value and then gradually declines.

In the LISC mode, the fracture behaviors are heavily influenced by the surface notches. Specifically, as shown in figure 6(d), as radial cracks propagate away from the ISC site, crack bifurcation is promoted by the perpendicular notches, which leads to the complete separation of the damaged area from the far field. Therefore, a major portion of the electrode was not involved in ISC, resulting in a reduced heat generation. Compared with the reference cell, the temperature increase of modified cell is drastically lowered and the post-peak temperature reduction is considerably faster (figure 3(b)). In fact, if the coin cell is fully discharged, when it is impacted, due to rupture, plastic deformation, and friction of cell components, there would still be a mild temperature rise (figure 3(c)). When the notch depth is 14 μm, ΔT of modified cell is only slightly higher than that of fully discharged reference cell by less than 1 °C, suggesting that heat generation of ISC is efficiently suppressed. With the temperature increase of the fully discharged reference cell being subtracted, the effective ΔT of modified cell with 14 μm deep notches is below 10% of that of reference cell.

The notch depth, D, is a critical factor. As summarized in figure 3(b), when D is 6 μm, the temperature increase of modified cell is only slightly lower than that of reference cell, ΔT_{ref}. Examination of the impacted electrodes indicates that while crack bifurcation occasionally occurs, the central damaged ISC area is never completely separated from the far field; all petals of the current collector between radial cracks are only deformed, not truncated (figures 6(b) and (c)). Hence, the path between the far field and the ISC site remains highly conductive. As the notch depth is increased to 10 μm, the average ΔT decreases by ~40%, yet the probability of GISC is still high (figure 3(d)). The temperature increase distribution becomes bimodal: ΔT is either quite close to ΔT_{ref} or much lower than it; no sample falls in between. Inspection on damaged electrodes reveals that the high-ΔT cells, about 50% of all the tested samples, fail in a similar way as the cells with D = 6 μm; that is, at least one deformed current-collector petal connects the central ISC area to the far field, so that the GISC mode is dominant. In the other ~50% cells, wall the current-collector petals are detached from the far field, so that the LISC mode dominates. Clearly, the heat generation is mostly affected by whether the separation of ISC site is complete. As the notch depth rises to 14 μm, in all the samples crack bifurcation causes the isolation of the central ISC areas (figure 6(d)). Hence, only the small central piece of electrode is involved in the discharge and contributes to the temperature increase, so that ΔT is close to that of fully discharged reference cell. Further increasing notch depth will not enhance the internal-shorting-mitigation performance, but incur processing difficulties.

The ultimate tensile strength, σ_{ts}, and the failure strain, ε_{f}, of modified current collector are dependent of the notch depth (figure 4(a)). The normalized notch depth is defined as $D^* = 1 - t_{\mathrm{r}}/t_0$, where t_{r} is the ligament length at notch root and t_0 is the initial current collector thickness. As D^* increases, both strength and ductility of current collect decrease monotonously. Figure 4(b) suggests that the failure work, $W = \int_0^{u_0} F\mathrm{d}u$, is sensitive to D, as it should be; here, F and u are the measured force and the displacement, respectively, and u_0 is the maximum displacement. Compared with

reference current collector wherein $D = 0$, when the notch depth reaches 35% of current-collector thickness (t_0), σ_{ts} and ε_f are reduced by ~1/2 and ~2/3, respectively; the work of tensile force, W, largely decreases by about 5 times. If D is further decreased to ~60% of t_0, W is lowered to only ~4% of that of reference current collector. The notch-induced brittleness greatly increases the probability of formation of a complete ring-shaped crack around the central ISC site; thus, in the impact test not only the mean value of ΔT but also its data scatter is reduced.

Figures 5 and 6 show that the simulated deformation and fracture modes of current collector agree well with the experimental observation. In the reference current collector, the deformed petals around the indenter are connected with the fringe area, providing charge transport paths and causing GISC. With 6 μm deep surface notches, the damage mode of current collector changes: Instead of random crack propagation, the cracks are guided by the notches from the indenter to the far field; however, no perimetric cracks are formed. As the notch depth increases to 10 μm, a portion of the petals are truncated through crack bifurcation; depending on whether the perimetric crack forms a complete loop, the cell behaviors can be dominated by either GISC or LISC. When D is 14 μm, full separation of ISC site always takes place; crack bifurcation leads to the formation of complete ring crack surrounding the indentation site and therefore, LISC becomes the governing mechanism.

Figure 7 demonstrates the stress distributions at various stages of impact. For the reference current collector, stress concentrate at the indentation site is evident; after cracking begins, plastic deformation zones (PDZ) at crack tips dominate the crack propagation along radial directions. With the surface notches, the stress field is highly heterogeneous. At the notch roots, the local stress is much higher than in adjacent areas. As the notches are relatively shallow, e.g. when $D = 6$ μm, the stress distribution is relatively homogeneous around the indenter. Hence, the fracture of current-collector petals is somewhat similar to the behavior of reference specimen. As the notches are relatively deep, e.g. when $D = 14$ μm, the notch root effects are evident and even in the near field the stress field is highly heterogeneous, resulting in the complete perimetric crack. The factor of notch depth comes in more critically by affecting the crack bifurcation.

4. Conclusions

To conclude, modifying current collector by surface notches can help mitigate thermal runaway of mechanically abused LIB cell, and the notch depth is a critical parameter. As the LIB cell is impacted, with relatively shallow notches, although radial cracks in current collector tend to advance along the notches, the petals in between the radial cracks are still partly connected to the far field, so that global internal short circuit (GISC) mode dominates. When the notches are sufficiently deep, the current collector becomes effectively brittle, and the failure work is drastically reduced. Due to the stress/strain concentration effect of surface notches, crack bifurcation is promoted and a complete perimetric crack ring can be generated, fully isolating the damaged area from the undamaged portion of the electrode. Consequently, the overall heat generation rate is considerably lowered. This finding opens the door to the development of robust multifunctional large-sized LIB cells.

Acknowledgement

This research was supported by the Advanced Research Projects Agency-Energy (ARPA-E) under Grant No. DE-AR0000396, for which we are grateful to Dr Ping Liu, Dr John Lemmon, Dr Grigorii Soloveichik, Dr Chris Atkinson, and Dr Dawson Cagle. Special thanks are also due to Professor Shirley Meng, Dr Hyojung Yoon, and Mr Minghao Zhang for their help with the battery cell processing.

ORCID iDs

Meng Wang https://orcid.org/0000-0001-9761-6802

References

[1] Diouf B and Pode R 2015 *Renew. Energy* **76** 375–80
[2] Li H and Zhou H 2012 *Chem. Commun.* **48** 1201–17
[3] Williard N, He W, Hendricks C and Pecht M 2013 *Energies* **6** 4682–95
[4] Wang Y W and Shu C M 2015 *Rechargeable Batteries, Green Energy and Technology* (Berlin: Springer) pp 419–54
[5] Karimi G and Li X 2013 *Int. J. Energy Res.* **37** 13–24
[6] Lu L, Han X, Li J, Hua J and Ouyang M 2013 *J. Power Sources* **226** 272–88
[7] Wang Q, Ping P, Zhao X, Chu G, Sun J and Chen C 2012 *J. Power Sources* **208** 210–24
[8] Balakrishnan P G, Ramesh R and Kumar T P 2006 *J. Power Sources* **155** 401–14
[9] Kennedy B, Patterson D and Camilleri S 2000 *J. Power Sources* **90** 156–62
[10] Zeng Z, Wu B, Xiao L, Jiang X, Chen Y, Ai X, Yang H and Cao Y 2015 *J. Power Sources* **279** 6–12
[11] Chen Z, Qin Y and Amine K 2009 *Electrochim. Acta* **54** 5605–13
[12] Wu B, Pei F, Wu Y, Mao R, Ai X, Yang H and Cao Y 2013 *J. Power Sources* **227** 106–10
[13] Zhang S S 2007 *J. Power Sources* **164** 351–64
[14] Huang X 2011 *J. Solid State Electrochem.* **15** 649–62
[15] Gao X, Sheng W, Wang Y, Lin Y, Luo Y and Li B G 2015 *J. Appl. Polym. Sci.* **132** 42169
[16] Zhong H, Kong C, Zhan H, Zhan C and Zhou Y 2012 *J. Power Sources* **216** 273–80
[17] Chen Z *et al* 2016 *Nat. Energy* **1** 15009
[18] Lisbona D and Snee T 2011 *Process Saf. Environ. Prot.* **89** 434–42
[19] Wang M, Le A V, Shi Y, Noelle D J, Wu D, Fan J, Lu W and Qiao Y 2017 *J. Appl. Phys.* **121** 015303
[20] Le A V, Wang M, Shi Y, Noelle D J and Qiao Y 2015 *J. Phys. D: Appl. Phys.* **48** 385501
[21] Wang M, Le A V, Shi Y, Noelle D J, Yoon H, Zhang M, Meng Y S and Qiao Y 2016 *J. Mater. Sci. Technol.* **32** 1117–21
[22] Liu P, Sherman E and Jacobsen A 2009 *J. Power Sources* **189** 646–50

[23] Zhao W, Luo G and Wang C Y 2015 *J. Electrochem. Soc.* **162** 1352–64
[24] Santhanagopalan S, Ramadass P and Zhang J Z 2009 *J. Power Sources* **194** 550–7
[25] Wang M, Le A V, Noelle D J, Shi Y, Yoon H, Zhang M, Meng Y S and Qiao Y 2016 *Int. J. Damage Mech.* at press (https://doi.org/10.1177/1056789516660176)
[26] Wang M, Le A V, Shi Y, Noelle D J and Qiao Y 2017 *Appl. Phys. Lett.* **110** 083902
[27] Wang M, Le A V, Noelle D J, Shi Y, Meng Y S and Qiao Y 2017 *J. Power Sources* **349** 84–93
[28] Wang M, Shi Y, Noelle D J, Le A V, Yoon H, Chung H, Zhang M, Meng Y S and Qiao Y 2017 *RSC Adv.* **7** 45662–7